ORIGINAL ARTICLE

An analysis of the radiological factors associated with respiratory failure in COVID-19 pneumonia and the CT features among different age categories

Akito Fukuda[1,2] · Noriyo Yanagawa[3] · Noritaka Sekiya[4] · Koji Ohyama[1] · Makiko Yomota[2] · Takanori Inui[4] ·
Sho Fujiwara[1] · Shoko Kawai[2] · Kazuaki Fukushima[1] · Masaru Tanaka[1] · Taiichiro Kobayashi[1] · Keishiro Yajima[1] ·
Akifumi Imamura[1]

Abstract

Purpose To investigate CT patterns of COVID-19 pneumonia associated with respiratory failure (RF) focused on the distribution of lesions.

Materials and methods Eighty-five patients with COVID-19 pneumonia were reviewed. CT findings were classified as follows: Type A; patchy ground glass attenuation (GGA) with/without air-space consolidation, Type B; non-segmental GGA with/without air-space consolidation in both the central and peripheral lung portions especially with subpleural spare, and Type C; non-segmental GGA with/without air-space consolidation predominantly distributed in the peripheral lung portion without subpleural spare. We analyzed CT patterns and clinical factors associated with RF, including age categories.

Results The number of patients with Type A, B and C was 31 (37%), 24 (28%) and 30 (35%), respectively. Type C and hypertension were independently associated with RF. On comparing between Types B and C, the frequency of traction bronchiectasis was higher in Type C than in Type B ($P < 0.001$). The ratio of Type C in patients ≥ 65 years old (66%) was higher than in patients < 40 years old ($P < 0.001$) and 40–49 years old ($P = 0.001$).

Conclusion The Type C, increasing with age, was associated with RF. Traction bronchiectasis in the lesion was more frequent in Type C than in Type B.

Secondary abstract

A lesion adjacent to the pleura and hypertension is associated with respiratory failure in patients with COVID-19. The frequency of a lesion adjacent to the pleura increased with age. The distribution of lesions is a useful parameter to predict respiratory failure.

Keywords COVID-19 · SARS-CoV-2 · Pneumonia · Respiratory failure · Computed tomography

✉ Noritaka Sekiya
  qnmnk410@ybb.ne.jp

1 Department of Infectious Diseases, Tokyo Metropolitan Cancer and Infectious Diseases Center Komagome Hospital, Tokyo, Japan

2 Department of Respiratory Medicine, Tokyo Metropolitan Cancer and Infectious Diseases Center Komagome Hospital, Tokyo, Japan

3 Department of Radiology, Tokyo Metropolitan Cancer and Infectious Diseases Center Komagome Hospital, Tokyo, Japan

4 Department of Infection Prevention and Control, Department of Clinical Laboratory, Tokyo Metropolitan Cancer and Infectious Diseases Center Komagome Hospital, 3-18-22 Hon-komagome, Bunkyo-ku, Tokyo 1138677, Japan

Introduction

The novel coronavirus infection initially broke out in Wuhan, China, and rapidly spread across the globe [1]. Pneumonia is a major complication of COVID-19 and strongly associated with an unfavorable prognosis [2]. Previous studies have shown that COVID-19 infections are more likely to be severe illness in patients with underlying conditions and comorbidities, such as obesity, diabetes mellitus, hypertension, hyperlipidemia, hyperuricemia, COPD, asthma, and chronic renal disease [3, 4]. Age and sex are also essential prognostic factors associated with this disease, with older men more likely to experience a severe course [3, 4].

Several reports have analyzed the CT findings correlated with the severity of pneumonia, including widespread lesions, consolidation, crazy-paving appearance, pleural effusion, dilatation bronchi, air bronchogram, vessel enlargement, and the involvement of the upper lobe or right middle lobe [5–7]. A previous report evaluated whether or not CT findings differ by age, with the frequency of large lesions or bilateral lesions in patients over 45 years old found to be significantly higher than in patients under 18 years old. This report showed that the tendency for older patients to have more widespread lesions than younger patients is one factor associated with the poor prognosis in older patients [9].

We have noticed that previously undescribed features of peripheral subpleural located ground glass opacities/consolidation seemed to be associated with the disease severity. Certain CT findings have been observed in numerous patients with SARS-CoV-2 pneumonia in our clinical practice. We therefore focused on the distribution of pulmonary lesions, including their previously undescribed features, and evaluated the relationship between the distribution of these lesions and the severity of respiratory failure as well as the differences in the distribution of lesions across age groups.

Materials and methods

Study design and data collection

A retrospective cohort study was conducted at a tertiary-care cancer and infectious diseases center in Japan. Patients with COVID-19 admitted to our hospital from Mar 1 to Apr 20, 2020, who underwent CT on admission or during hospitalization were included. COVID-19 was diagnosed by positive for severe acute respiratory syndrome coronavirus 2 (SAR-Cov-2) polymerase chain reaction (PCR) of the nasopharyngeal or pharygeal swab. Three patients with no abnormal opacity and one patient with diffuse abnormal opacifications due to silicosis were excluded.

The patient characteristics, coexisting conditions, including hypertension, diabetes, cardiovascular disease, chronic obstructive pulmonary disease, and cancer; laboratory findings on admission; and CT findings were collected using electronic medical records.

The institutional review board of Komagome Hospital approved the present study (IRB number 2531).

CT examinations

All patients were scanned with a 64-MDCT scanner (Aquillion ONE; Tokyo, Japan) from the thoracic inlet to the diaphragm while at full inspiration without contrast medium. The scan was carried out with the following settings: 0.5-mm collimation; 120 kV; auto-exposure control; gantry

rotation time of 0.5 s; and beam pitch of 0.83. All images were reconstructed using standard reconstruction at a slice thickness of 5 mm and an interval of 7 mm in the whole lung field and using a high-resolution algorithm with a slice thickness of 0.5 mm and an interval of 0.5 mm in the entire lung field. Images were observed at window settings appropriate for the parenchyma (window width, 1200–1500 HU; window level, −700 to −600 HU) and mediastinum (width, 300–400 HU; level 30–60 HU) on high-resolution liquid crystal diode monitors.

Imaging interpretation

Two board-certified radiologists (N.Y., chest radiologist with 24 years of experience; T.I., general radiologist with 9 years of experience) independently reviewed the initial CT scans in random order and reached consensus by discussion when their judgements differed. CT images were evaluated for the radiological patterns, and the extension of abnormal opacities (< 50% or ≥ 50%) in the whole lung. To compare the CT findings in the pulmonary lesion between Types B and C, air-space consolidation, traction bronchiectasis, and intralobular and/or interlobular septal thickening were evaluated in both groups. CT patterns were divided into three groups based on the distribution of the lesion, as follows:

- Type A (Fig. 1): patchy round-shaped ground-glass attenuation (GGA) or GGA plus air-space consolidation with a 10–40-mm diameter. This radiological pattern was assumed to represent the early stages of infection.
- Type B (Fig. 2, 3): the lesions are formed by the confluence of the patchy GGA with or without air-space consolidation and have lobulated margins, being distributed

Fig. 1 A 36-year-old man with COVID-19 pneumonia (Type A). Axial CT image (lung window) at the level of the lower lobe. Round-shaped patchy ground glass attenuation was visualized in the bilateral lower lobe
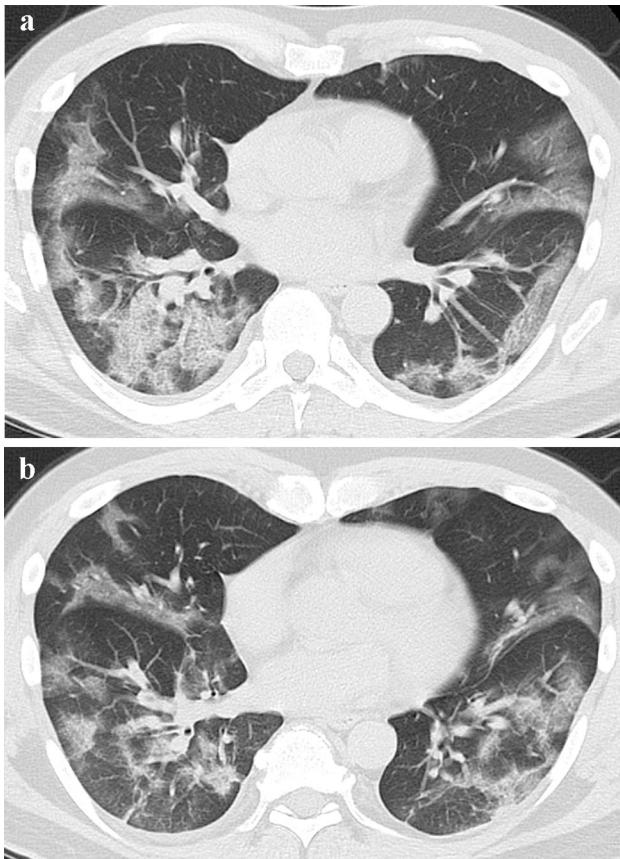
Fig. 2 A 51-year-old man with COVID-19 pneumonia (Type B). **a**, **b** Axial CT image (lung window) at the level of the lower lobe. Non-segmental ground glass attenuation was visualized in the bilateral lungs. The lesions were distributed predominantly subpleural portion without subpleural spared areas

Fig. 3 A 71-year-old man with COVID-19 pneumonia (Type B). Axial CT images (lung window) at the level of the upper lobe (**a**) and lower lobe (**b**). Non-segmental ground glass attenuation was visualized diffusely in the bilateral lungs. Most lesions were distributed in the central area of the lung with subpleural spared areas

non-segmentally in both the central and peripheral portions of the lung. There are variable-width subpleural spared areas in most portions, which is one of the essential features of this type.

- Type C (Fig. 4): non-segmental GGA with or without air-space consolidation predominantly distributed in the peripheral portion of the lung and suspected to have been formed by extension along the pleura from an early stage. There are no subpleural spared areas, which is an essential finding of Type C that differentiates it from Type B.

When multiple patterns were mixed, the pattern with the widest lesion area was defined as the main pattern. The timing of the CT scan and the oxygen demand (≥ 5 L) from the onset of symptom were assessed for each CT type. The extension of lesions ($< 50\%$ or $\geq 50\%$) in the whole lung was estimated by the visual assessment on two different CT views (axial and coronal views using multi-planar reconstruction).
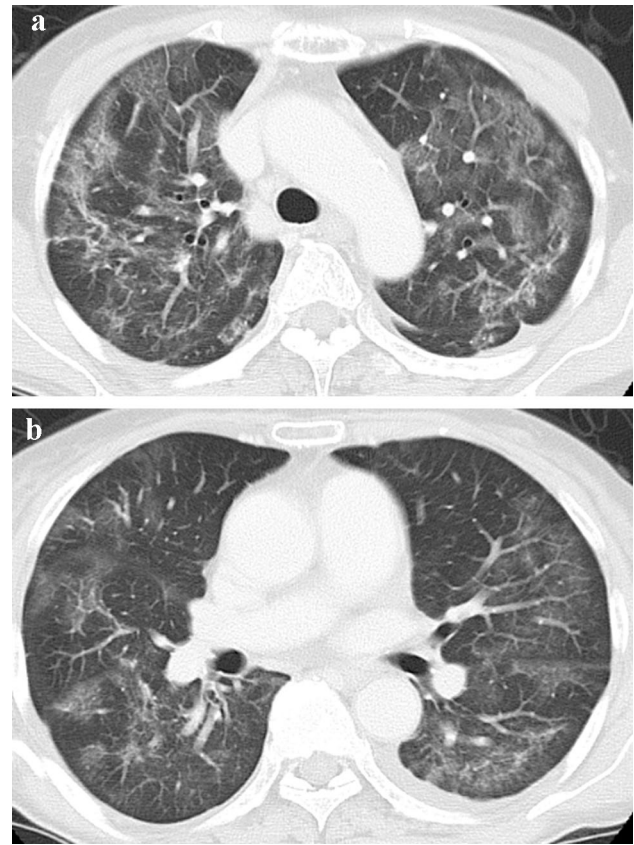
Ground-glass attenuation (GGA) was defined as an area of hazy increased opacification without obscuration of underlying vascular markings. Air-space consolidation was defined as increased opacification with vascular markings.

Data analyses

- Analysis of the clinical, laboratory, and radiological factors related to respiratory failure (RF)

  First, we divided subjects into two groups based on the maximum oxygen demand for evaluation as a primary outcome according to the WHO guidance [10]: RF group, ≥ 5 L; non-RF group, < 5 L. The presence or absence of RF was judged for the period that was presumed to be the peak period across the entire course of each case. We analyzed which factors (clinical findings, laboratory data, and CT patterns) correlated with RF using multivariate analysis. The clinical findings and laboratory data for this analysis were selected based on variables previously reported to be poor prognostic factors. Because the lesion extent has been reported as a risk
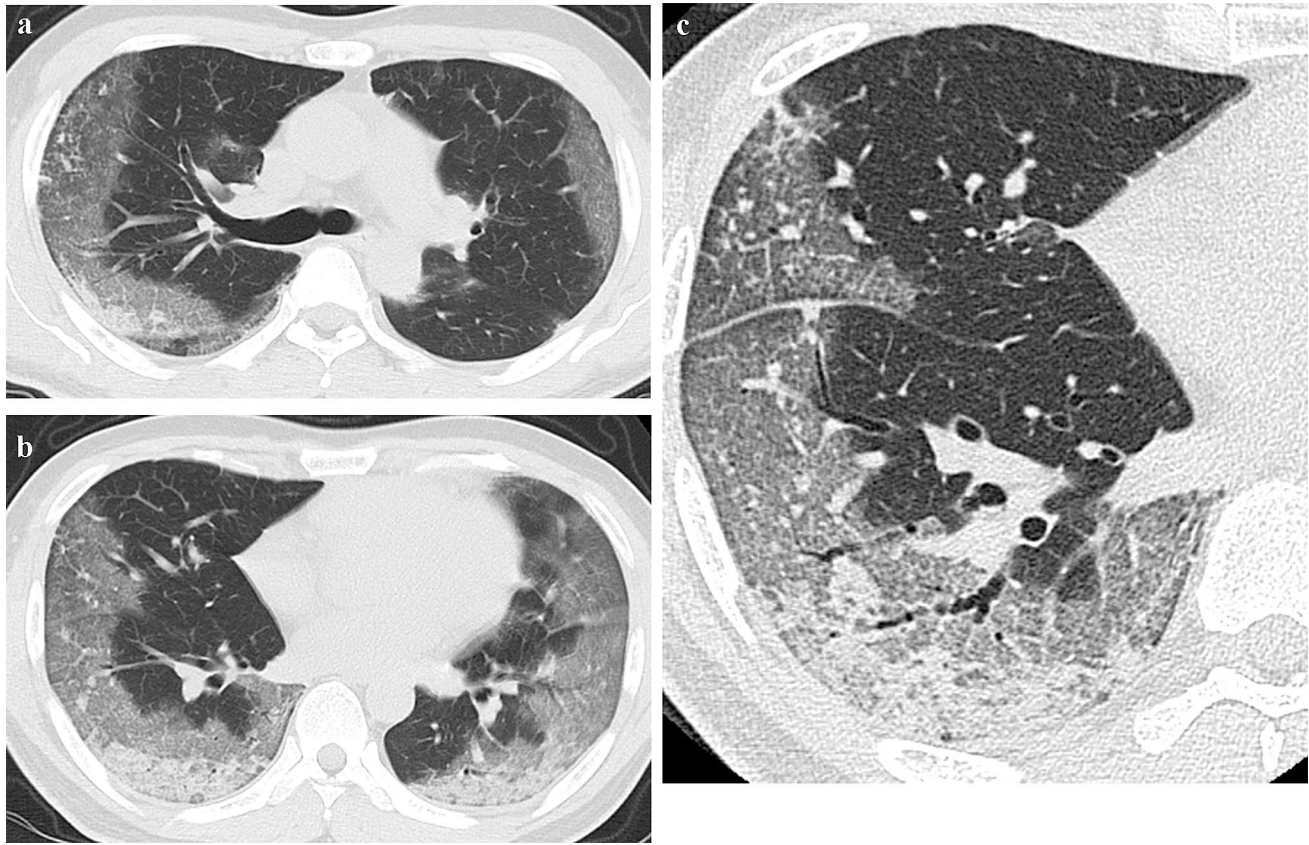
Fig. 4 A 53-year-old man with COVID-19 pneumonia (Type C). Axial CT images (lung window) at the level of the upper lobe (**a**) and lower lobe (**b**, **c**). Non-segmental ground glass attenuation was visualized in the bilateral lungs, distributed adjacent to the pleura. Traction bronchiectasis was seen in the lesion (**c**)

factor for disease severity, we checked for differences between groups in the proportion of cases with a lesion extent ≥ 50%.

- The comparison CT findings in pulmonary lesions between Types B and C

To determine whether or not there was a difference in CT findings between Types B and C, both of which included cases with a lesion extent ≥ 50%, the frequency of three CT findings (air-space consolidation, traction bronchiectasis, and interlobular and/or intralobular septal thickening) was evaluated. The three CT findings were selected based on reports describing the CT findings of acute interstitial pneumonia (AIP) [9, 9].

- The evaluation of the clinical tendency in Type C patients and the evaluation of the relationship between CT type and age

We evaluated the duration from the initial CT examination to the development of RF in Type C patients. To assess the relationship between the radiological type and age, the subjects were divided into 4 groups according to age (< 40 years old, 40–49 years old, 50–64 years old, ≥ 65 years old). The classification by age was based on the Centers for Disease Control and Prevention's (CDC) report concerning COVID-19 hospitalizations and death by age [4].

Statistical analyses

Statistical analyses were performed using EZR version 1.40. Categorical and continuous variables were evaluated with Fisher's exact test using Bonferroni's correction when necessary and the Mann–Whitney U test, respectively. The Kruskal–Wallis test was used to compare CT types. We considered variables with a P value of < 0.05 in the univariate analysis to be candidate variables for inclusion in the multivariate logistic regression model.

Results

Patient characteristics

Of the 89 patients who underwent CT during the study period, 85 (male, 62; median age, 57 years old, range

22–95 years old) were included in the analysis. The clinical characteristics and laboratory data of all subjects are summarized in Table 1. The severity of patients based on the WHO guidance was as follows: moderate (49 cases, 58%), severe (15 cases, 18%), and critical (21 cases, 25%) [11].

CT findings

The kappa statistic for the diagnosis of the CT pattern was 0.830, and the inter-observer agreement was very good.

The number (%) of patients with a CT pattern of Types A, B and C was 31 (37), 24 (28) and 30 (35), respectively (Table 1). The time (median [interquartile range]) from the onset of symptoms to the CT examination in Types A, B and C was 8.0 days (5.0–14.0), 9.5 days (8.0–12.0) and 8.0 days (5.0–11.0), respectively. There were no significant differences among the groups (P=0.186).

The number of patients (%) with ≥50% lesion extension in Types A, B and C were 0 (0%), 4 (16%) and 8 (26%),

respectively. The ratio of Type C cases with ≥50% lesion extension was higher than that the ratio of Type A cases (P=0.001). In contrast, there were no significant differences in the ratio of cases with the ≥50% lesion extension between the Type B and C groups (P=0.515).

Clinical, laboratory and radiological factors related to RF

The number of RF and non-RF patients (%) was 30 (35) and 55 (65), respectively. The results of the analysis are summarized in Table 2. In the univariable analysis, age, sex, hypertension, C-reactive protein, lactate dehydrogenase, d-dimmer, serum ferritin were factors associated with RF. In the multivariable analysis, Type C and hypertension were factors independently associated with RF.

Table 1 Patient characteristics of each CT type

	Total $N=85$	Type A $N=31$ (37)	Type B $N=24$ (28)	Type C $N=30$ (35)
Age (years)				
<40	14 (16)	14(45)	0 (0)	0 (0)
40–49	12 (14)	4 (13)	7 (29)	1 (3)
50–64	30 (35)	8 (26)	12 (50)	10 (33)
65 ≤	29 (34)	5 (16)	5 (21)	19 (63)
Sex (male)	62 (73)	24 (77)	13 (54)	25 (83)
Severity				
Moderate	49 (58)	26 (84)	13 (54)	10 (33)
Severe	15 (17)	2 (6)	8 (33)	5 (17)
Critical	21 (25)	3 (10)	3 (13)	15 (50)
Brinkman Index ≥ 400	15 (18)	5 (16)	1 (4)	9 (30)
Comorbidity				
Hypertension	25 (29)	7 (23)	5 (21)	13 (43)
Diabetes	18 (21)	4 (13)	3 (16)	11 (37)
Cardiovascular Disease	6 (7)	3 (10)	0 (0)	3 (10)
Chronic obstructive pulmonary disease	4 (4)	0 (0)	0 (0)	4 (13)
Cancer	11 (13)	1 (3)	2 (8)	8 (27)
Laboratory data				
White cell count—per mm^3	5300 (4200–6200)	4900 (4100–6250)	5450 (4675–5850)	5600 (4300–6725)
C-reactive protein—mg/dL	3.4 (1.4–10.92)	1.5 (0.4–2.7)	5.0 (2.1–7.2)	10.9 (3.5 –17.3)
Lactate dehydrogenase > 245 U/L	63 (74)	13 (42)	23 (96)	27 (90)
D-dimmer > 1 mg/L	35 (41)	10 (32)	4 (17)	21 (70)
KL—6 > 500 U/mL	11 (13)	1 (3)	2 (8.0)	8 (27)
Serum ferritin > 300 ng/mL	44 (52)	9 (29)	11 (46)	24 (80)
Respiratory failure	30 (35)	2 (6)	3 (13)	25 (83)
Days from the onset of symptoms	8.0 (6.0–12.0)	8.0 (5.0–14.0)	9.5 (8.0–12.0)	8.0 (5.0–11.0)

Data are presented as the number (%) or median (interquartile range)

Table 2 The association between RF and the clinical/radiological features

	Total N=85	RF N=30	Non-RF N=55	Univariable OR (95% CI)	P value	Multivariable aOR (95% CI)	P value
Age ≥ 65	28 (33)	15 (50)	13 (24)	3.2 (1.1–9.3)	0.017		
Sex (male)	62 (73)	27 (90)	35 (64)	5.1 (1.3–29.3)	0.01		
Brinkman Index ≥ 400	15 (18)	7 (32)	8 (16)	2.5 (0.6–9.4)	0.129		
Comorbidity							
Hypertension	25 (29)	15 (50)	10 (18)	4.4 (1.5–13.7)	0.003	21.7 (2.2–217.0)	0.009
Diabetes	18 (21)	10 (33)	8 (15)	2.9 (0.9–9.9)	0.06		
Cardiovascular disease	6 (7)	3 (1)	3 (5)	1.9 (0.2–15.2)	0.66		
Chronic obstructive pulmonary disease	4 (4)	3 (10)	1 (2)	5.9 (0.5–320.0)	0.12		
Cancer	11 (13)	7 (23)	4 (7)	3.8 (0.87–19.6)	0.05		
Laboratory data							
White cell count—per mm^3		5700 (4625–7225)	5200 (4100–6050)	1.0 (1.0–1.0)	0.11		
C-reactive protein—mg/dL		10.2 (5.09–17.3)	1.9 (0.8–4.3)	1.2 (1.1–1.3)	<0.001		
Lactate dehydrogenase > 245 U/L	63 (74)	28 (93)	35 (64)	7.8 (1.7–77.8)	0.004		
D-dimmer > 1 mg/L	35 (41)	19 (63)	16 (29)	3.5 (1.2–10.0)	0.011		
KL—6 > 500 U/mL	11 (13)	6 (20)	5 (6)	2.4 (0.5–11.3)	0.19		
Serum ferritin > 300 ng/mL	44(52)	25 (83)	19 (22)	12.3 (3.1–72.4)	<0.001		
CT type							
Type A vs. Type B	31 vs. 24	2 (6) vs. 3 (13)	29 (94) vs. 21 (87)	2.0 (0.2–26.5)	0.643		
Type C vs. Type B	30 vs. 24	25 (83) vs3 (13)	5 (17) vs. 21 (87)	31.6 (6.3–231.4)	<0.001	117.3 (9.8–1400.6)	<0.001
Type C vs. Type A	30 vs. 31	25 (83) vs. 2 (6)	5 (17) vs. 29 (94)	64.0 (11.1–738.2)	<0.001	157.9 (12.8–1953.1)	<0.001

Data are presented as the number (%) or median (interquartile range)

RF respiratory failure, *OR* odds ratio, *aOR* adjusted OR, *CI* confidence interval

The comparison of CT findings in pulmonary lesions between Types B and C

The number and frequency of the three CT findings assessed are summarized in Table 3. Although the frequency of air-space consolidations and interlobular and/or intralobular septal thickening did not differ markedly between the two groups, the frequency of traction bronchiectasis was significantly higher in Type C than in Type B (Fig. 4c).

The evaluation of the clinical tendency in Type C patients and the evaluation of the relationship between radiological type and age

Among the Type C patients, 94% had developed RF within 5 days of the CT scan being performed.

The proportions of CT patterns among different age groups (< 40 years old, 40–49 years old, 50–64 years old, ≥ 65 years old) are shown in Fig. 5. All patients < 40 years old had Type A. The main radiological

Table 3 Comparison of CT findings in the pulmonary lesions between Type B and Type C

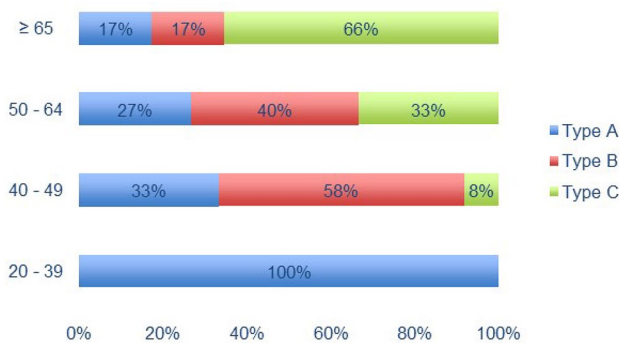| CT findings	CT pattern		P value
	Type B ($n=24$)	Type C ($n=30$)	
Air-space consolidation	16 (67%)	17 (57%)	0.453
Traction bronchiectasis	2 (8%)	17 (57%)	< 0.001
Interlobular and/or intralobular septal thickening	15 (63%)	24 (80%)	0.154

Fig. 5 Trends in CT patterns by age. All patients who were < 40 years old showed Type A. The main radiological pattern in patients 40–49 years old was Type B. The frequency of Type C increased with age, and the ratio of Type C was significantly higher than patients ≥ 65 years old compared with patients < 50 years old

pattern in patients 40–49 years old was Type B (58%). The frequency of the Type C pattern increased with age, and the ratio of Type C among the patients ≥ 65 years old (66%) was significantly higher than among the patients < 40 years old and 40–49 years old ($P < 0.001$ and $P = 0.001$, respectively; using adjusted significance level after Bonferroni correction).

Discussion

This study highlights the significance of the Type C CT pattern, which is a risk factor associated with RF that demonstrates an increasing frequency with age. Older patients reportedly tend to have more widespread lesions than younger ones, and a wide lesion extent is significantly associated with a poor prognosis in COVID-19 infection [7]. Type A reflects early lesions, whereas Types B and C are CT patterns seen once the initial lesion has progressed, resulting in a wider lesion extent in Types B and C than in Type A.

According to previous reports that the extent of the lesion correlates with the severity of the disease, Types B and C should both be associated with a higher risk of RF than Type A. However, in the present study, only Type C was associated with RF. We speculate that the subpleural distribution may be a causative factor associated with RF. Several articles have described the histopathological findings of COVID-19 pneumonia, including diffuse alveolar damage (DAD), pneumocyte hyperplasia/necrosis, interstitial lymphoid infiltrate and organizing pneumonia (OP)/acute fibrinous and organizing pneumonia (AFOP), and these coexist in varying proportions within the lesion [10–13]. DAD is the most important pathological finding and strongly associated with a severe disease state. A previous report described the analysis of the distribution of pulmonary perfusion among patients with COVID-19 pneumonia using dual-energy CT. In that report, perfusion abnormality was found in 96% of cases, with 52% of cases showing increased pulmonary perfusion in the lesion and 96% showing decreased pulmonary perfusion in the lesion. Interestingly, all lesions that presented with decreased pulmonary perfusion were peripheral lung lesions [14]. Decreased pulmonary perfusion reflects oligemia, which may be closely associated with not only the consequence of DAD but also a factor in the development of DAD. Vascular damage may be more substantial in the subpleural area than in other pulmonary areas, so DAD may be more likely to present and occur in subpleural lesions than in other lesions. The frequency of traction bronchiectasis was significantly higher in Type C than in Type B. Traction bronchiectasis is a finding that occurs as a result of pulmonary volume loss due to fibrosis or organization and is associated with either the proliferative or fibrotic phase of DAD [9, 9]. A previous report compared the CT findings of AIP in survivors and non-survivors, and the extent of pulmonary lesions associated with traction bronchiectasis was found to be greater in non-survivors than in survivors [15]. The pathologic hallmark of AIP is the presence of DAD, and DAD can be categorized into three phases: acute exudative, subacute proliferative, and chronic fibrotic phase. Traction bronchiectasis is a finding not seen in the acute exudative phase, so a significant difference in the frequency of traction bronchiectasis between in Type B and in Type C does not mean that Type B has less DAD than Type C. It is possible that Type B has more lesions in the acute exudative phase of DAD, but in the present study, the CT images in the two groups were taken at almost the same time after the onset of disease, suggesting that the difference in the frequency of traction bronchiectasis in the pulmonary lesion may reflect the difference in the frequency of DAD rather than the difference in the timing of the lesion onsets.

It is presumed that not only DAD but also other factors contribute to the differing risk of RF depending on the distribution of lesions. Type B is characterized by subpleural curve linear opacity, which is lined up on the medial side of the pleura. The lymphatic flow in the lungs is divided into the hilar and pleural flow just below the medial line to the pleura. A previous report described the role of the pulmonary lymphatics in lung injury, noting that lymphatics had an overall protective effect against lung injury and fibrosis [16]. The difference in the direction of lymphatic flow may affect the recovery of pulmonary lesions, but the exact location of the change in the direction of lymphatic flow is unclear radiologically and there are no reports of differences in the direction of lymphatic flow affecting the recovery of pulmonary lesions, so the precise answers remain unclear at present.

Older patients were shown to be more likely to develop lesions distributed in area adjacent to the pleura, a tendency that has been reported previously [5]. Although the physiological changes in the lungs due to age may have influenced the differences in the distribution tendency, the exact reason for this is unknown.

Several limitations associated with the present study warrant mention. First, mild cases were excluded because we focused on patients receiving CT scans. Second, the timing of CT scans was varied. However, the median duration from the onset of symptoms was similar among types. Third, the CT type was difficult to determine in two cases because of mixed patterns. As we classified the cases according to our criteria, the validation of our classification approach is needed.

Conclusion

The Type C pattern on CT images was shown to be associated with RF. The frequency of Type C increased with age, and the ratio of Type C was significantly higher than patients ≥ 65 years old compared with patients < 50 years old. We believe that the distribution of lesions is a useful parameter to assess, as it can facilitate the prediction of and preparation for RF.

Declarations

Conflict of interest The authors have no conflicts of interest to disclose.

References

1. Zhu N, Zhang D, Wang W, et al. China novel coronavirus, T. Research, A novel coronavirus from patients with pneumonia in China, 2019. N Engl J Med. 2020;382:727–33.
2. Guan WJ, Ni ZY, Hu Y, H W, et al. China Medical Treatment Expert Group for, clinical characteristics of coronavirus disease 2019 in China. N Engl J Med. 2020;382:1708–20.
3. National institute of infectious disease, Japan, Descriptive epidemiology of 287 confirmed cases of new coronavirus infection reported by the national epidemiological surveillance of infectious disease system (NESID) and active epidemiological surveillance (as of Mar 9, 2020) https://www.niid.go.Jp/niid/ja/covid-19/9533-covid19-14-200323.html (Accessed Nov 1 2020)
4. Centers for disease control and prevention US Coronavirus disease 2019(COVID-19) People with certain medical conditions. https://www.cdc.gov/coronavirus/2019-ncov/need-extra-precautions/people-with-medical-conditions/html#asthma (Accessed Nov 1 2020)
5. Meiler S, Schaible J, Poschenrieder F, et al. Can CT performed in the early disease phase predict outcome of patient with COVID-19 pneumonia? Analysis of cohort of 64 patients from Germany. Eur J Radiol. 2020;131:109256.
6. Li Y, Yang Z, Ai T, et al. Association of "initial CT" findings with mortality in older patients with coronavirus disease 2019 (COVID-19). Eur Radiol. 2020;30:6186–93.
7. Chon YJ, Kim JY, Suh YJ, et al. Adverse initial CT findings associated with poor prognosis of coronavirus disease. J Korean Med Sci. 2020;35:e316.
8. Chen Z, Fan H, Cai J, et al. High-resolution computed tomography manifestations of COVID-19 infections in patients of different ages. Eur J Radiol. 2020;126:108972.
9. Ichikado K, Johkoh T, Ikezoe J, et al. Acute interstitial pneumonia: high-resolution CT findings correlated with pathology. Am J Roentgenol. 1997;168:333–8.
10. Andrew GN, Michael O, Anand D, et al. COVID-19 related lung pathology: old patterns in new clothing? Histopathology. 2020;77:169–72.
11. Copin MC, Parmentier E, Duburcq T, et al. Time to consider histologic pattern of lung injury to treat critically ill patients with COVID-19 infection. Intensive Care Med. 2020;46:1124–6.
12. Zhang H, Zhou P, Wei Y, et al. Histopathologic changes and SARS-CoV-2 immunostaining in the lung of a patient with COVID-19. Ann Intern Med. 2020;172:629–32.
13. Polak SB, Van Gool IC, Cohen D, et al. A systematic review of pathological findings in COVID-19:a pathophysiological timeline and possible mechanisms of disease progression. Mod Pathol. 2020;33:2128–38.
14. Lang M, Som A, Carey D, et al. Pulmonary vascular manifestations of COVID-19 pneumonia. Radiol Cardiothorac Imaging. 2020;2:e200277.
15. Johkoh T, Muller NL, Taniguchi H, et al. Acute interstitial pneumonia: comparison of high-resolution computed tomography findings between survivors and nonsurvivots. Am J Respir Crit Care Med. 2002;165:1551–6.
16. Baluk P, Naikawadi RP, Kim S, et al. Lymphatic proliferation ameliorates pulmonary fibrosis after lung injury. Am J Pathol. 2020;190:2355–75.